Chemistry of Polyfunctional Molecules, 129[◇]

Synthesis and X-Ray Structures of Novel Lead(1+) and Indium(3+) Phosphazenide Complexes; Detailed ^{207}Pb-NMR Spectra of the ^{207}Pb-Labelled Dimeric Lead(1+) Species

Astrid Winkler[a], Walter Bauer*[b], Frank W. Heinemann[a], Veronica Garcia-Montalvo[a][+], Matthias Moll[a], and Jochen Ellermann*[a]

Institut für Anorganische Chemie der Universität Erlangen-Nürnberg[a],
Egerlandstrasse 1, D-91058 Erlangen, Germany
Fax: (internat.) +49(0)9131/85-7367

Institut für Organische Chemie der Universität Erlangen-Nürnberg[b],
Henkestrasse 42, D-91054 Erlangen, Germany
Fax: (internat.) +49(0)9131/85-9132
e-mail: bauer@organik.uni-erlangen.de

Received November 10, 1997

Keywords: Lead(1+) / Indium(3+) / Organylphosphanylamide complexes / Phosphazene / ^{207}Pb-NMR spectra

The reaction of $PbCl_2$ with $LiN(PPh_2)_2$ (**1**) at −78°C affords the P−P coupled phosphazene $Ph_2P-N{=}PPh_2-PPh_2{=}N-PPh_2$ (**2**) as an oxidation product and, as a reduction equivalent, the novel lead(1+) complex $[(Pb^{1+})_2(\mu\text{-}Ph_2P{=}N{=}PPh_2^-)_2](Pb-Pb)$ (**3**). The crystal structure determination of the red compound **3** shows a Pb−Pb bond length of 304.1(1) pm. The ^{31}P- and ^{207}Pb-NMR spectra of **3** are complicated due to the presence of a higher order spin system (AA′A′′A′′′X for the mono-^{207}Pb isotopomer, AA′A′′A′′′XX′ for the bis-^{207}Pb isotopomer). Simulations of the ^{31}P and ^{207}Pb spectra both on material with natural isotope abundance and on the ^{207}Pb-labelled compound (**3***) reveal a large Pb,Pb coupling constant of 7708 Hz, indicative of a covalent Pb−Pb bond. − Though $InCl_3$ is diagonally related to $PbCl_2$, no significant redox process is observed in the reaction between $InCl_3$ and **1**. The yellow crystals of $[In^{3+}(Ph_2P{=}N{=}PPh_2^-)_3]$ (**4**) that are obtained were also investigated by X-ray analysis. These show a propeller-like configuration of the three four-membered chelate rings with indium(3+) as the centre.

Previously[2][3][4] we published data on the unusual *oxidative splitting* and scrambling of lithium bis(diphenylphosphanyl)amide, $LiN(PPh_2)_2$ (**1**)[5][6][7][8], by MCl_2 (M = Co, Fe, Ni, Pd, Pt) that resulted in spirocyclic[2][3] and bicyclic[4] complexes of the types A, B, and C (Scheme 1). In contrast, the *oxidative coupling* of **1** with iodine[9] leads to the P−P coupled diphosphazene $Ph_2P-N{=}PPh_2-PPh_2{=}N-PPh_2$ (**2**), that can also be obtained by the reaction of **1** with anhydrous iron(3+) fluoride, copper(2+) fluoride[10], bismuth tribromide or antimony triiodide[11]. On the other hand, a mixture of arsenic triiodide and **1** in the molar ratio of 1:2 reacts at 20°C to yield **2** and the As(1+) complex D[11].

As a part of our studies on the chemical behaviour of **1** towards metal halides, we now report on the reaction of **1** with $PbCl_2$ and $InCl_3$, the latter having a diagonal relationship with $PbCl_2$.

Scheme 1

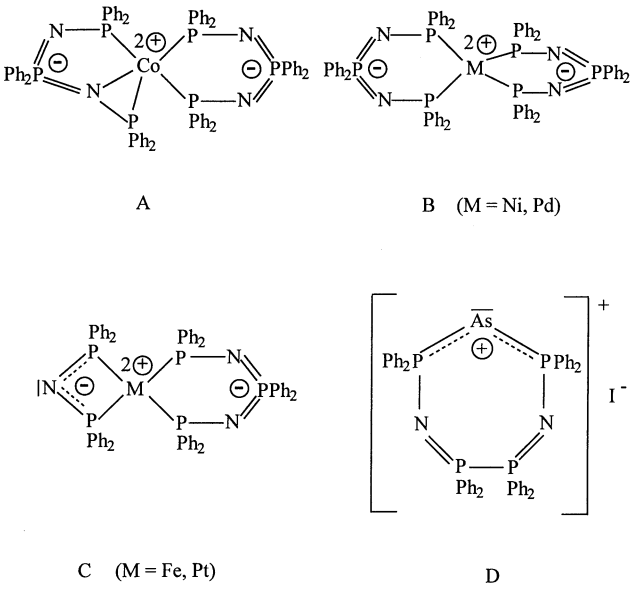

The Binuclear Lead(1+) Complex

The reaction of lead dichloride with two equivalents of **1** at −78°C, allowed to warm up to 20°C, in THF affords the diphosphazene **2** and a new complex, **3,** with lead in the rare oxidation state of 1+ (Scheme 2).

[◇] Part 128: Ref.[1].
[+] Present address: Instituto de Quimica, Universidad Nacional Autonoma de Mexico, Circuito Exterior, Ciudad Universitaria, 04510, Mexico D. F. (Mexico).

  1434−1948/98/437−444 $ 17.50+.50/0

Scheme 2

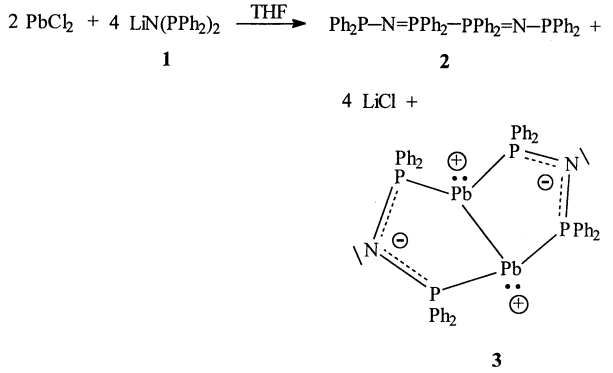

Compounds **2** and **3** can be isolated as pale yellow and deep red crystals, respectively, from THF by precipitation with *n*-pentane. In order to separate **2** and **3,** the crystal conglomerate was treated with cold toluene, in which **3** dissolves. Compound **2** was filtered off and identified by infrared spectroscopy[11].

Crystallization of **3** from toluene by slow solvent diffusion with *n*-pentane yielded large red rhombic crystals which were suitable for X-ray structural analysis.

The result of the structure determination of **3** is shown in Figure 1. The molecule contains a $[Pb^{1+}-Pb^{1+}]$ unit with an interatomic distance of 304.1(1) pm, which is considerably shorter than the interatomic Pb···Pb distance (349 pm)[12] in metallic lead. This indicates the possibility of a covalent $Pb^{1+}-Pb^{1+}$ bond in **3**, and this is confirmed by the ^{207}Pb-NMR spectrum of the ^{207}Pb-labelled **3** (= **3***) which shows a large ^{207}Pb,^{207}Pb coupling constant of 7708 Hz (see later). In the polylead anions Pb_5^{2-}, Pb_7^{4-}, Pb_9^{4-}, and in organometallic diplumbanes of type $R_3Pb-PbR_3$ (R = Ph, *c*-C_6H_{11}) Pb−Pb distances in the range of 284−324 pm are found[13]. The Pb(1)−Pb(2) bond of **3** is bridged by two bis(diphenylphosphanyl)amide anions, $[N(PPh_2)_2]^-$, forming a butterfly-like structure with P(1)−Pb(1)−P(4) and P(2)−Pb(2)−P(3) angles of 93.7(2)° and 95.5(2)°, respectively. All other angles at the Pb(1) and Pb(2) atoms also approach the "p-only" value of 90°. Therefore, the two vicinal lone electron pairs at the lead atoms (Scheme 2) have mainly s-character.

The average P−N bond length of 160(2) pm, which is typical for complexes with the *bridging* $[N(PPh_2)_2]^-$ entity[14][15][16], indicates a considerable amount of double-bond character. The two five-membered rings connected by the Pb(1)−Pb(2) bond show significant deviations from planarity (Figure 2). Whereas in the Pb(1)−P(1)−N(1)−P(2)−Pb(2) ring the P(1) atom is displaced by 30 pm from the least-squares plane, the deviation for the P(3) atom in the homologous Pb(1)−P(4)−N(2)−P(3)−Pb(2) ring is 26 pm. The dihedral angle between the two least-squares planes calculated for the two five-membered rings amounts to 89.4°. The P−N−P angles of 123.4(9)° and 125.2(11)°, respectively, are the same as those found in $(THF)_3LiN(PPh_2)_2$ [124.7(3)°][8].

Figure 1. Molecular structure (ORTEP plot) of **3**[a]

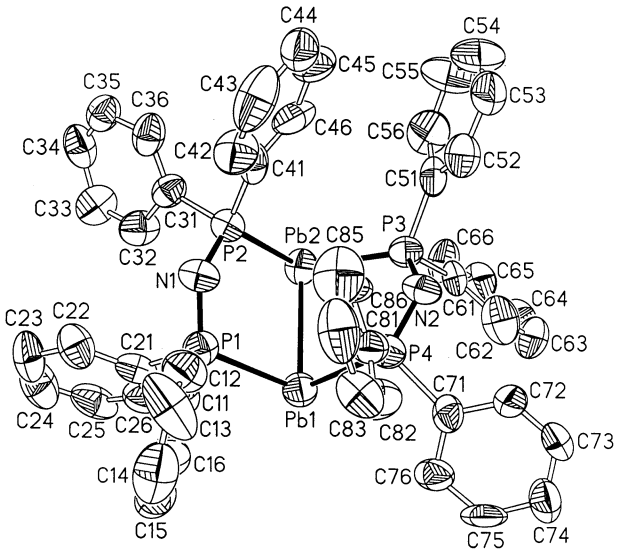

[a] Selected bond lengths [pm] and angles [°]: Pb(1)−P(1) 273.6(6), Pb(1)−P(4) 278.0(6), Pb(1)−Pb(2) 304.10(13), Pb(2)−P(3) 270.9(6), Pb(2)−P(2) 274.0(6), P(1)−N(1) 160(2), P(1)−C(11) 180(2), P(1)−C(21) 181(2), P(2)−N(1) 160(2), P(3)−N(2) 163(2), P(4)−N(2) 158(2); P(1)−Pb(1)−P(4) 93.7(2), P(1)−Pb(1)−Pb(2) 84.94(13), P(4)−Pb(1)−Pb(2) 88.93(12), P(3)−Pb(2)−P(2) 95.5(2), P(3)−Pb(2)−Pb(1) 84.32(12), P(2)−Pb(2)−Pb(1) 88.30(12), C(11)−P(1)−C(21) 99.7(10), N(1)−P(1)−Pb(1) 116.9(7), C(11)−P(1)−Pb(1) 113.6(8), C(21)−P(1)−Pb(1) 105.6(8), N(2)−P(3)−Pb(2) 120.1(7), N(2)−P(4)−Pb(1) 114.6(7), P(1)−N(1)−P(2) 123.4(9), P(4)−N(2)−P(3) 125.2(11).

Figure 2. Arrangement and distortion of the five-membered rings in **3**

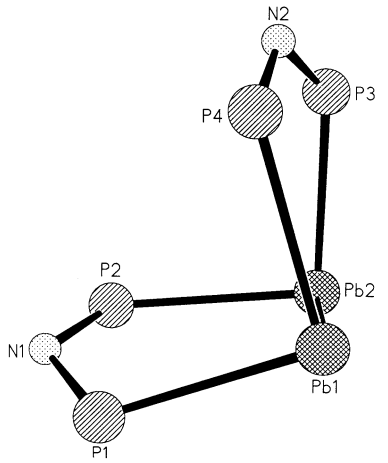

^{31}P- and ^{207}Pb-NMR Spectra

Whereas phosphorus is an element consisting of a pure isotope (100% ^{31}P, spin $I = 1/2$), lead consists of only 22.4% of the isotope ^{207}Pb (spin $I = 1/2$). Other stable lead isotopes are magnetically inactive (spin $I = 0$). Hence, according to the binomial coefficients, the natural isotope abundance distribution in **3** is 61%, 34%, and 5% for the presence of zero, one, and two ^{207}Pb isotopes, respectively.

The skeleton of magnetically active P and Pb nuclei in **3** is shown in Figure 3. For the sake of convenience we use the numbering shown in Figure 3 in the following discussion. In

the trivial case of the major isotopomer in which no ^{207}Pb isotope is present, the four ^{31}P nuclei are equivalent and give rise to a singlet at $\delta = 60.7$ in the ^{31}P-NMR spectrum (c.f. Figure 4). In the isotopomer shown in Figure 3a, with one ^{207}Pb isotope, an AA′A′′A′′′X spin system (A = A′ = A′′ = A′′′ = ^{31}P; X = ^{207}Pb) is present which results in rather complex ^{31}P and ^{207}Pb spectra (Figures 4a and 5a). Of crucial interest is the isotopomer with the lowest abundance, in which two ^{207}Pb nuclei are present (Figure 3b): here, an AA′A′′A′′′XX′ spin system exists with complex ^{31}P and ^{207}Pb spectra that are entirely different from those arising from the presence of only one ^{207}Pb isotope (Figures 4b and 5b).

Figure 3. Skeleton of magnetically active P and Pb nuclei in **3**. a) Isotopomer with one ^{207}Pb; b) isotopomer with two ^{207}Pb

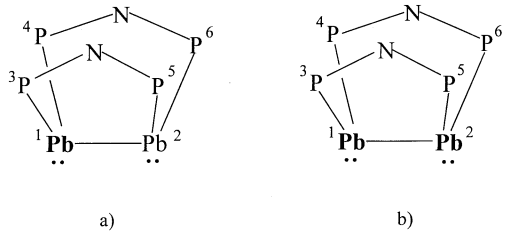

Figure 4. Simulated (a−c) and experimental (d) ^{31}P-NMR spectrum of **3**, natural isotope abundance, C_6D_6, satd. solution, +23°C. Spectrum (c) is a superposition of spectrum (a) (mono-^{207}Pb isotopomer) and spectrum (b) (bis-^{207}Pb isotopomer) with scaling to the appropriate isotopomer abundances. Signals in spectrum (d) which do not match the signals of the simulated spectrum are due to impurities from thermal decomposition

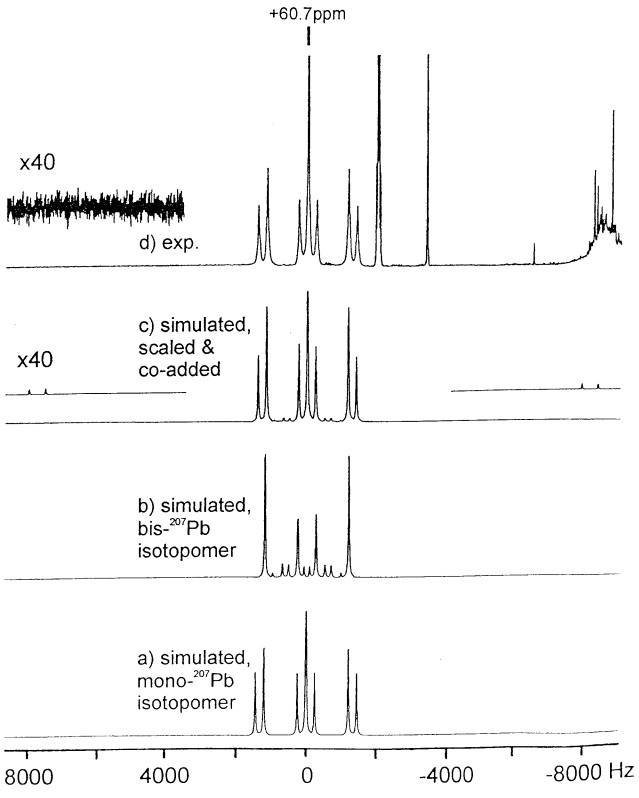

In order to elucidate the coupling constants involved, the ^{31}P- and ^{207}Pb-NMR spectra were simulated for the isotopomers with one and with two ^{207}Pb nuclei (Figures 4 and 5). The simulated spectra were scaled according to the abundances of the isotopomers and superimposed (Figures 4c and 5c). The corresponding experimental spectra are shown in Figures 4d and 5d. The ^{31}P- and ^{207}Pb-chemical shifts are $\delta = 60.7$ and $\delta = -608.0$, respectively. It should be noted that the simulation software employed cuts off signals below a certain intensity. Hence, simulations by using different software may reveal additional weak signals.

Figure 5. Simulated (a−c) and experimental (d) ^{207}Pb-NMR spectrum of **3**, natural isotope abundance, C_6D_6, satd. solution, +23°C. Spectrum (c) is a superposition of spectrum (a) (mono-^{207}Pb isotopomer) and spectrum (b) (bis-^{207}Pb isotopomer) with scaling to the appropriate isotopomer abundances

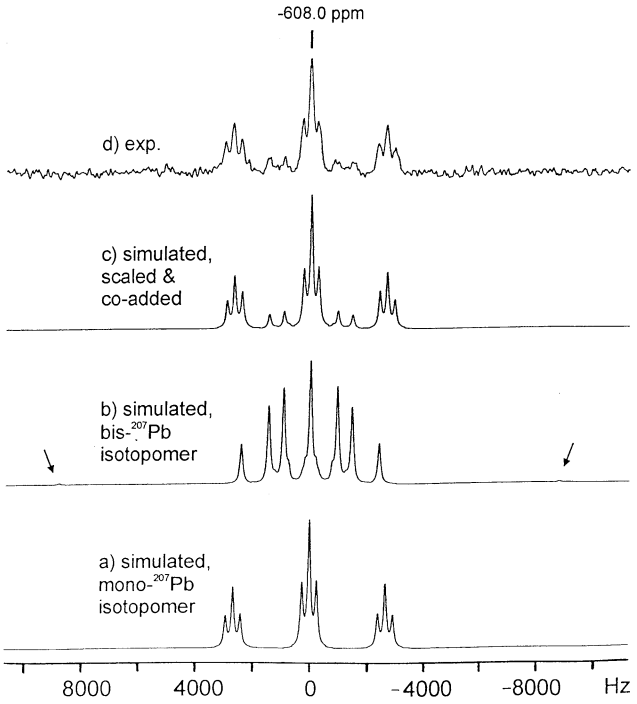

The coupling constants J_{13}, J_{15}, and J_{35} were relatively easily determined after some variation cycles. By contrast, the coupling constant "of interest", J_{12}, manifests only as very weak "satellites", which are visible in the simulation only after a large zoom of the vertical scale (Figures 4c and 5b). Variation of J_{12} over a wide range results in no significant changes in the center "multiplet". In the experimental ^{31}P and ^{207}Pb spectra of the natural abundance material these satellites are completely lost in the spectrum noise.

The simulated spectra are not sensitive to the sign of the homonuclear couplings J_{12} and J_{35} (J_{46}). Permutations of the signs of these coupling constants resulted in absolutely identical spectra. Hence, it is not possible to determine the signs of these coupling constants from the simulations. In contrast, the simulated spectra are sensitive to the relative signs of the heteronuclear coupling constants J_{13} and J_{15}. The simulations clearly indicate that the signs of J_{13} and J_{15} are unlike. Although many one bond (^1J)Pb,Pb couplings have been measured[17], the sign has been determined only recently[18] for a larger variety of compounds. Thus, J_{12} is

negative throughout for, e.g., tBu$_3$Pb-PbR$_3$ (R = Me, Et, iPr, n-C$_6$H$_{11}$, c-C$_6$H$_{11}$) and amounts up to −9200 Hz for R = n-C$_6$H$_{11}$. Only in Pb$_2$Me$_6$ J_{12} has been found to be positive[19]. It is save to assume that J_{12} is negative in **3**, especially when the influence of the 6s electron pairs is taken into account[20][21]. Tentatively, we hold the same to be true for J_{13} in **3**. Accordingly, the geminal coupling constant J_{15} must be positive.

In order to make visible the very weak "satellite" signals which are indicative of the Pb,Pb coupling constant in **3**, we carried out isotopic labelling. The synthesis of the labelled material is shown in Scheme 3. The ^{207}Pb-labelled compound is referred to as **3*** in the following text.

Scheme 3

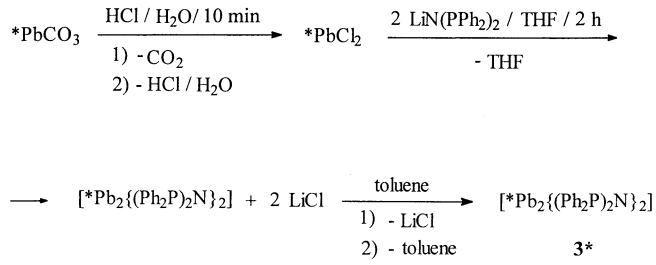

The ^{207}Pb enrichment of the initially employed ^{207}PbCO$_3$ is 92.8%. Hence, the distribution of the isotopomers of **3*** with zero, one, and two ^{207}Pb nuclei is 0.5%, 13.3%, and 86.2%, respectively. As for the ^{31}P- and ^{207}Pb-NMR measurements of the natural abundance material, crystals of **3*** were dissolved in [D$_6$]benzene. Due to the limited thermal stability of **3*** the ^{31}P spectrum (Figure 6d) is blurred due to the presence of signals from decomposition products. Unfortunately, these overlap heavily with the "satellite" signals of interest (Figure 6c) which would be indicative of the magnitude of the Pb,Pb coupling. Hence, even for the ^{207}Pb-labelled compound the relevant constant J_{12} could not be extracted from the ^{31}P spectrum.

Fortunately, however, the ^{207}Pb spectrum of **3*** (Figure 7d) finally yielded the desired information. The overall measuring time of this ^{207}Pb spectrum was 126 h. Spectra of several freshly prepared samples were superimposed. Although ^{207}Pb is generally a nucleus that is easy to detect, the broadness of the signals generally leads to a poor signal-to-noise ratio. This broadness is very likely due to chemical shift anisotropy (CSA) relaxation, a well known phenomenon with high field spectrometers[22]. When the simulation is carried out using the Pb,Pb coupling constant $|J_{12}|$ = 7708 Hz, the outer satellites in Figures 7b and 7c match the experimentally observed ones in Figure 7d.

Table 1 summarizes the results of the spin simulations. Diagonal numbers represent chemical shifts whereas off-diagonal numbers indicate coupling constants.

The large Pb,Pb coupling constant of 7.7 kHz clearly indicates that a covalent Pb−Pb bond must be present in **3**. Therefore, complex **3** bears a remote resemblance to [Ge$_2${C(SiMe$_3$)(PMe$_2$)$_2$}$_2$], which contains a covalent Ge−Ge bond[23].

Figure 6. Simulated (a−c) and experimental (d) ^{31}P-NMR spectrum of **3***, isotopically labelled by 92.8% ^{207}Pb, C$_6$D$_6$, satd. solution, +23°C. Spectrum (c) is a superposition of spectrum (a) (mono-^{207}Pb isotopomer) and spectrum (b) (bis-^{207}Pb isotopomer) with scaling to the appropriate isotopomer abundances. Signals in spectrum (d) which do not match the signals of the simulated spectrum are due to impurities from thermal decomposition

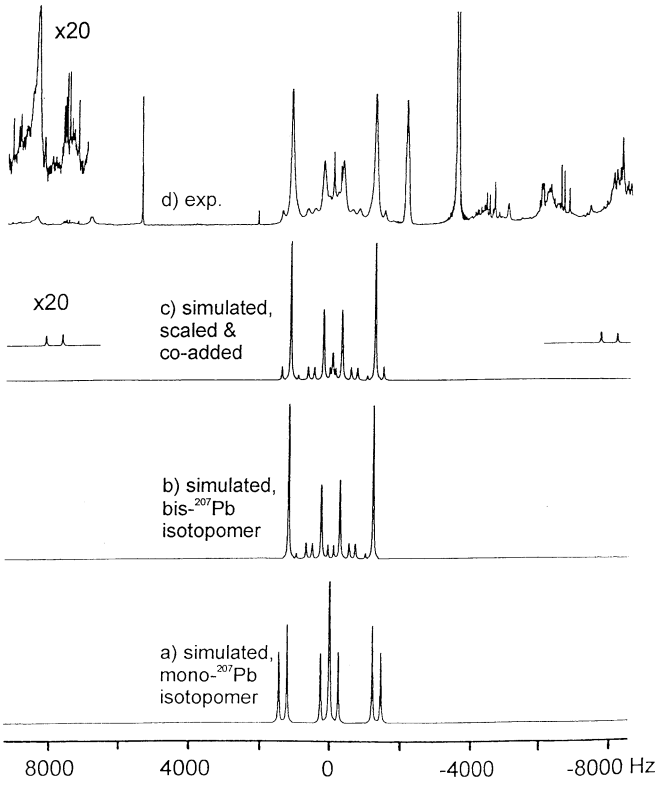

The ^{1}H-NMR spectrum of **3** is simple and does not have any unusual features. As a result of P,C coupling, the resonances for C-i and C-o of the phenyl groups in the ^{13}C{^{1}H}-NMR spectrum are split into multiplets. The IR spectroscopic data of **3** are listed in the Experimental Section. The assignments of the P−C$_6$H$_5$ modes[6] are based on the Whiffen nomenclature[24] in the more currently used description of Maslowsky[25]. The mass spectrum (EI) of **3** does not show the molecular ion peak of **3**$^+$, but instead shows the [M − PPh] fragment along with various peaks due to P−N and P−Ph fragments.

It is also worth pointing out that ligands which are similar to our system, i. e. [N(SiMe$_3$)$_2$]$^-$, [N(SiMe$_3$)(CMe$_3$)]$^-$, [N(SPPh$_2$)$_2$]$^-$, and [CH(PPh$_2$)$_2$]$^-$ generally yield different complexes with the lower main group-15 metal(2+) halides, e. g. [Pb{N(SiMe$_3$)$_2$}$_2$][26], [Pb{N(SiMe$_3$)(CMe$_3$)}$_2$][27], [Sn{N(SiMe$_3$)$_2$}$_2$][28], [Pb{(SPPh$_2$)$_2$N}$_2$][29], [Sn{CH(PPh$_2$)$_2$}$_2$][30], or [Pb{CH(PPh$_2$)$_2$}$_2$][30][31][32].

The Mononuclear Indium(3+) Complex

Reaction of InCl$_3$ with LiN(PPh$_2$)$_2$ (**1**) in the molar ratio of 1:3 in THF at 20°C affords LiCl and the yellow complex [In(Ph$_2$P=N=PPh$_2^-$)$_3$] (**4**), which was isolated after separation from LiCl with benzene/n-pentane as yellow moisture-sensitive crystals. These crystals were suitable for an X-

Figure 7. Simulated (a−c) and experimental (d) ^{207}Pb NMR spectrum of **3***, isotopically labelled by 92.8% ^{207}Pb, C_6D_6, satd. solution, +23°C. Spectrum (c) is a superposition of spectrum (a) (mono-^{207}Pb isotopomer) and spectrum (b) (bis-^{207}Pb isotopomer) with scaling to the appropriate isotopomer abundances

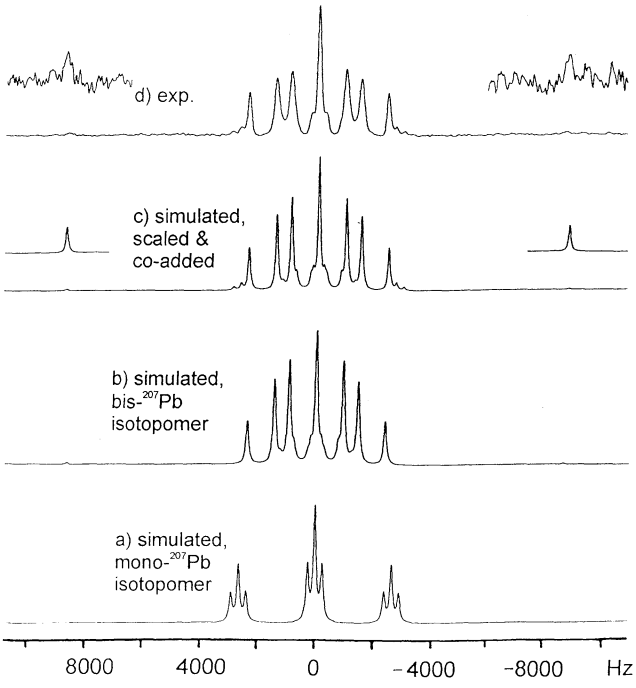

Table 1. ^{31}P- and ^{207}Pb-chemical shifts (δ, diagonal, ppm) and coupling constants (*J*, off-diagonal, Hz) in **3** and **3***, respectively, as derived from spectra simulations. The signs of the coupling constants are tentative (see text), however, it is certain that J_{13} (J_{14}, J_{25}, J_{26}) and J_{15} (J_{16}, J_{23}, J_{24}) have unlike signs

Nucleus #	1	2	3	4	5	6
1	−608.0	−7708	−2660	−2660	+240	+240
2		−608.8	+240	+240	−2660	−2660
3			+60.7	0	+240	0
4				+60.7	0	+240
5					+60.7	0
6						+60.7

ray crystal analysis. Surprisingly there is no reduction of $InCl_3$ to indium(1^+) derivatives by **1**.

The crystal structure determination shows that compound **4** consists of a tricyclic ring system with indium(3+) as the centre (Figure 8).

At the indium centre the four-membered P−N−P−In chelate rings are oriented in a propeller-like conformation. The main deviation from a regular octahedral arrangement is caused by the fact that the P−In−P angle for each bidentate $[N(PPh_2)_2]^-$ ligand is close to 58°. In the four-membered ring In(1)−P(3)−N(2)−P(4), the differences between the two P−N and In−P bond lengths as well as the two In−P−N angles are small. These differences in the related bond distances and angles increase in the In(1)−P(1)−N(2)−P(2) ring and are remarkable in the In(1)−P(5)−N(3)−P(6) ring [e.g. P(5)−N(3): 167.3(6), P(6)−N(3): 158.7; In(1)−P(5): 284.7(2), In(1)−P(6): 273.9(2) pm; In(1)−P(5)−N(3): 91.8, In(1)−P(6)−N(3): 97.9(2)°]. Accordingly, the tris(chelate) **4** does not contain a threefold symmetry axis and shows only C_1 symmetry. This clearly demonstrates that an octahedral or trigonal prismatic coordination polyhedron is not expected for **4**. The stereochemistry of complexes with coordination number 6 depends mainly on the normalized bite "*b*" of the bidentate ligand[33], which is defined in the case under discussion as *b* = P···P/In−P (distance between the donor atoms of the chelate/metal-donor atom distance). For the three four-membered rings mentioned above the *average* and normalized bites "*b*" are 1.02, 1.01, and 1.03, respectively. They are near the lowest limit known to date for tris(chelate) complexes with four-membered rings (*b* = 1.05 to 1.25)[33], e.g. $[Co(Ph-N=N-N-Ph^-)_3]$[34] *b* = 1.07[33]. The exceptional structure of **4** has no relationship with regular coordination polyhedras and is therefore best described as "propeller-like". The average value of the P−N bond lengths is 164.0(6) pm, and this is typical for complexes with the *chelating* $[N(PPh_2)_2]^-$ entity[4] and indicates π-electron delocalization.

Figure 8. Molecular structure (ORTEP plot) of **4**[a]

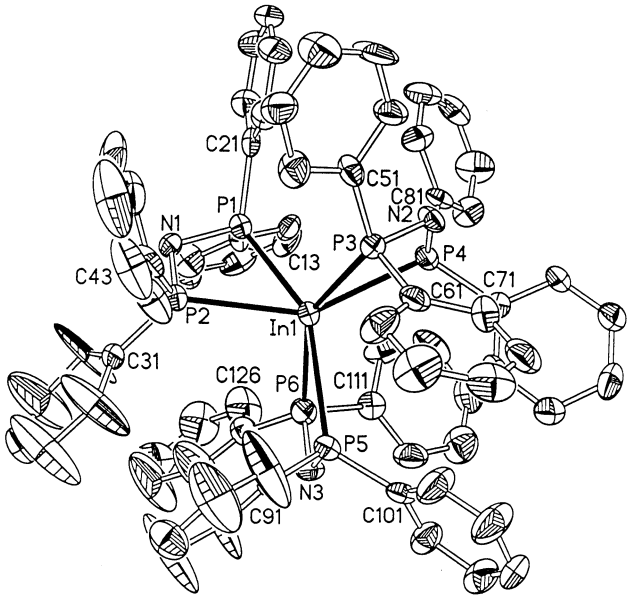

[a] Selected bond lengths [pm] and angles [°]: In(1)−P(1) 272.4(2), In(1)−P(6) 273.9(2), In(1)−P(4) 277.0(2), In(1)−P(2) 277.5(2), In(1)−P(3) 279.5(2), In(1)−P(5) 284.7(2), P(1)−N(1) 164.5(6), P(1)−C(21) 180.4(9), P(1)−C(11) 182.1(8), P(2)−N(1) 162.9(6), P(3)−N(2) 165.2(5), P(4)−N(2) 165.7(6), P(5)−N(3) 167.3(6), P(6)−N(3) 158.7(6), P(1)···P(2) 270.5(3), P(3)···P(4) 272.9(3), P(5)···P(6) 270.2(3); P(1)−In(1)−P(6) 101.14(7), P(1)−In(1)−P(4) 96.69(7), P(6)−In(1)−P(4) 106.61(6), P(1)−In(1)−P(2) 58.93(6), P(6)−In(1)−P(2) 99.34(6), P(4)−In(1)−P(2) 147.65(7), P(1)−In(1)−P(3) 105.26(7), P(6)−In(1)−P(3) 150.96(7), P(4)−In(1)−P(3) 58.71(6), P(2)−In(1)−P(3) 104.48(7), P(1)−In(1)−P(5) 149.72(7), P(6)−In(1)−P(5) 57.80(7), P(4)−In(1)−P(5) 109.65(6), P(2)−In(1)−P(5) 100.35(6), P(3)−In(1)−P(5) 101.17(7), N(1)−P(1)−C(21) 108.8(3), N(1)−P(1)−C(11) 109.3(3), C(21)−P(1)−C(11) 102.7(4), N(1)−P(1)−In(1) 95.3(2), C(21)−P(1)−In(1) 124.3(3), N(1)−P(2)−In(1) 93.8(2), N(2)−P(3)−In(1) 93.9(2), N(2)−P(4)−In(1) 94.7(2), N(3)−P(5)−In(1) 91.8(2), N(3)−P(6)−In(1) 97.9(2), P(2)−N(1)−P(1) 111.4(3), P(3)−N(2)−P(4) 111.1(3), P(6)−N(3)−P(5) 111.9(4).

Because it was impossible to record an IR spectrum in KBr under nitrogen, the air moisture caused sample decomposition during scanning, resulting in formation of $HN(PPh_2)_2$ (**5**) and decolorization. Compound **5** was identified by its IR spectrum[6]. It was not possible to anneal NMR tubes and so the NMR spectra of **4** contain signals of the impurity **5**.

This work was supported by the *Deutsche Forschungsgemeinschaft*, the *Fonds der Chemischen Industrie*, and the *Zerweck-Fonds* of the University of Erlangen-Nuernberg. We are also grateful to Prof. Dr. *D. Sellmann* for technical support concerning the X-ray analyses. We thank Prof. Dr. *B. Wrackmeyer* for valuable discussions. Dr. *V. Garcia-Montalvo* acknowledges *CONACYT* (Consejo Nacional de Ciencia y Tecnologia, México) for a post doctoral visiting fellowship.

Experimental Section

General: All operations were carried out under an atmosphere of pre-purified dry dinitrogen using standard Schlenk and vacuum line techniques. Solvents were dried and purified prior to use by conventional methods. Chemicals of the best available commercial grade were used: *n*-butyllithium (1.6 M solution in *n*-hexane, Merck-Schuchardt), $PbCl_2$ (Aldrich), $^{207}PbCO_3$ (Campro Scientific), $InCl_3$ (Aldrich). $HN(PPh_2)_2$ (**5**) was prepared according to literature procedures[6][35]. − IR: Perkin Elmer 983. − The NMR spectra of **3** and **3*** were recorded on a JEOL Alpha 500 spectrometer (11.7 Tesla) at 104.7 MHz (^{207}Pb) and 202.4 MHz (^{31}P), respectively. ^{207}Pb-NMR spectra are referenced to $Pb(NO_3)_2$ $\delta = -2961$ as a secondary reference ($PbMe_4$ $\delta = 0$). ^{31}P-NMR spectra are referenced to 85% H_3PO_4. No corrections for bulk susceptibilities have been applied. Samples of natural abundance and isotopically labelled compounds were prepared as saturated solutions of crystalline material in C_6D_6. Measurements were carried out at +23°C. A multinuclear 5 mm probehead was employed. ^1H-broadband decoupling was applied throughout. Samples were non-spinning. Spectral widths were 60 kHz (^{207}Pb) and 38 kHz (^{31}P), respectively. Recycle delays were 5 s (^{207}Pb) and 2.5 s (^{31}P). Pulse widths were 90° (13 μs, ^{207}Pb) and 60° (8 μs, ^{31}P). Measuring times were 43 h (Figure 4), 258 h (Figure 5), 20 h (Figure 6), and 126 h (Figure 7). Due to the thermal instability of **3** and **3***, the spectra of several freshly prepared samples were superimposed. Spectrum simulations were performed using the COMIC software package (JEOL). A Lorentzian line width of 30 Hz was used to match the experimental spectra. NMR of **4**: JEOL JNM-GX-270 (269.60 MHz for ^1H, 69.70 MHz for $^{13}C\{^1H\}$, 109.40 MHz for $^{31}P\{^1H\}$). Chemical shifts are relative to solvent signals, which in turn are referenced to TMS; for $^{31}P\{^1H\}$ NMR, 85% H_3PO_4 was employed as external standard. − MS: Varian MAT 212 (70 eV). − Microanalyses: Carlo Erba 1106 and 1108. − Melting points (uncorrected): Electrothermal IA 6304.

Preparation of Bis-μ-[bis(diphenylphosphanyl)amido-P,P']dilead(1+)(Pb−Pb) (**3**) *and Separation from 1.1.3.3.4.4.6.6-Octaphenyl-2.5-diaza-1.6-($\sigma^3\lambda^3$)diphospha-3.4-($\sigma^4\lambda^5$)diphosphahexane* (**2**): To a solution of 1.72 g (4.47 mmol) of $HN(PPh_2)_2$ (**5**) in 35 ml of THF was added 2.80 ml (4.48 mmol) of *n*-butyllithium (1.6 M solution in *n*-hexane) and the mixture was stirred for 30 min at −78°C. After addition of 0.62 g (2.23 mmol) of solid $PbCl_2$ and removal of the refrigerant, the colour of the suspension slowly changed from light yellow to deep red, while the mixture became a clear solution. Stirring was continued for 3 h at 20°C, then one third of the solvent was removed in vacuo. The residual clear deep red solution was layered with 85 ml of *n*-pentane and kept at 20°C for 5 d; deep red rhombic crystals of **3** and yellow cubes of **2** crystallized simultaneously. The two compounds were separated by decanting the solvent mixture of THF and *n*-pentane and treating the crystal conglomerate with cold toluene. While **3** dissolved, **2** was filtered off, washed with cold toluene and dried in vacuo to yield 0.45 g (52%). Mp. 155°C, mp.[10] 157°C.

Recrystallization of **3** from toluene by slow solvent diffusion (*n*-pentane) techniques afforded large red rhombic crystals after 3 d at 20°C; yield 0.84 g (63%), m.p. 140°C (dec.).

$Ph_2P-N=PPh_2-PPh_2=N-PPh_2$ (**2**): IR (KBr): $\tilde{\nu} = 3080\ cm^{-1}$ (w sh) + 3055 (w-m), 3030 (vw), 3025 (w) + 3010 (vw sh) [ν(CH)], 1586 (w-m) [ν(CC)k], 1568 (w) [ν(CC)l], 1475 (m) [ν(CC)m], 1431 (s) [ν(CC)n], 1389 (w) [2 × ϕ(CC)v], 1313 (w sh) + 1303 (w-m) [ν(CC)o], 1275 (w-m) [δ(CH)e], 1185 (vs), 1170 (vs) [ν(P=N)] + 1160 (s sh) [δ(CH)c], 1102 (m-s) [P^{IV}−Ph sens. q], 1090 (s) [P^{III}−Ph sens. q], 1068 (m) [δ(CH)d], 1027 (m) [δ(CH)b], 999 (w-m) [γ ring p, Ph], 975 (w) [γ(CH)j], 935 (vw) [γ(CH)h], 920 (w-m) [γ(CH)i], 848 (w) [γ(CH)g], 745 (s) [γ(CH)f], 720 (m-s), 714 (m-s) [P^{IV}−Ph sens. r], 699 (s) [P^{III}−Ph sens. r], 691 (m-s) [ϕ(CC)v], 661 (m-s) [ν(P−P) + γ(PNP)], 619 (w) + 605 (sh) [δ(CCC)s], 519 (m-s), 508 (s), 490 (m-s) [P−Ph sens. y], 458 (m-s), 441 (m) [P−Ph sens. t], 410 (w), 397 (w) [γ(CC)w], 382 (m), 371 (m) [δ(PNP)].

(**3**): IR (KBr): $\tilde{\nu} = 3070\ cm^{-1}$ (w-m sh) + 3055 (m), 3005 (w), 2990 (vw) [ν(CH)], 1585 (w-m) [ν(CC)k], 1570 (w-m) [ν(CC)l], 1478 (m) [ν(CC)m], 1432 (s) [ν(CC)n], 1385 (w) [2 × ϕ(CC)v], 1330 (w), 1305 (w) [ν(CC)o], 1275 (w) [δ(CH)e], 1180 (w-m) [δ(CH)a], 1159 (w-m) [δ(CH)c], 1128 (s) [ν(P⩬N)], 1105 (m-s), 1099 (m-s), 1088 (m-s) [P−Ph sens. q + ν(P⩬N)], 1070 (w-m) + 1048 (w) [δ(CH)d], 1026 (m) [δ(CH)b], 999 (w-m) [γ ring p, Ph], 970 (w) [γ(CH)j], 930 (vw) [γ(CH)h], 918 (vw) [γ(CH)i], 884 (w-m, br) [ν(P−N)], 850 (w) [γ(CH)g], 780 (m) [ν(P−N)], 748 (m), 738 (m-s) [γ(CH)f], 699 (vs) + 692 (s sh) [P−Ph sens. r + ϕ(CC)v], 620 (w), 603 (w) [δ(CCC)s], 555 (w), 548 (w-m) [γ(P⩬N⩬P)], 520 (vs), 490 (w-m), 480 (m) [P−Ph sens. y], 457 (w-m), 426 (m), 411 (w-m) [P−Ph sens. t], 376 (w), 358 (vw) [δ(NP_2)]. − ^1H NMR (C_6D_6, 21°C): δ = 6.45−6.90 (m, aromatic H). − $^{13}C\{^1H\}$ NMR (C_6D_6, 25°C): δ = 127.84 (s, C-*m*, Ph), 127.93 (s, C-*m*, Ph), 128.65 (s, C-*p*, Ph), 129.42 (s, C-*p*, Ph), 131.61 (m, C-*o*, Ph), 132.38 (m, C-*o*, Ph), 140.6 (m, C-*i*, Ph), 144.1 (m, C-*i*, Ph). − $^{31}P\{^1H\}$ NMR (C_6D_6, 22°C): δ = 58.9 (s). − EI-MS (70 eV, ref. to ^{208}Pb): *m/z* (%): 1076 (0.04) [M^+ − PPh], 768 (25) [**2**$^+$], 691 (6) [**2**$^+$ − Ph], 597 (65) [$(Ph_2PN)_3^+$], 583 (65) [$Ph_2P-N=PPh_2-N=PPh_2^+$], 520 (65) [$(Ph_2PN)_3^+$ − Ph], 460 (22) [$(Ph_2P)_2NPh^+$ − H], 384 (100) [$Ph_2P=N-PPh_2^+$], 306 (65) [$Ph_2P=N-Ph^+$], 262 (65) [PPh_3^+], 183 (92) [$(C_6H_4)_2P^+$], 122 (64) [$N\equiv P-Ph^+$]. − $C_{48}H_{40}N_2P_4Pb_2$ (1183.1): calcd. C 48.73, H 3.41, N 2.37; found C 49.14, H 3.45, N 2.38.

Preparation of [$^{207}Pb_2$(μ-$Ph_2P-N-PPh_2$−P,P')$_2$] (**3***): 0.155 g (0.580 mmol) of $^*PbCO_3$ was mixed with 12 ml of a concentrated aqueous solution of HCl. After the initially brisk foaming up had ceased the clear colourless solution was stirred for 10 min at 20°C. The solvent was removed under reduced pressure and the resulting $^*PbCl_2$ was dried at 100°C in vacuo for 4 h to exclude any traces of water. A conversion of 100% from $^*PbCO_3$ to $^*PbCl_2$ was assumed. 0.447 g of $HN(PPh_2)_2$ (**5**, 1.160 mmol) in 7 ml of THF was lithiated with 0.80 ml (1.280 mmol) of *n*-butyllithium (1.6 M solution in *n*-hexane), and the yellow solution was added to the solid $^*PbCl_2$ prepared as described above. After stirring for 2 h at 20°C the solvent from the red solution was evaporated in vacuo and the red residue was suspended in 7 ml of toluene for the separation of LiCl. Filtration with a D4 filter was followed by removal of the solvent from the filtrate to yield the red product [$^*Pb_2\{(Ph_2P)_2N\}_2$] that had traces of the by-product $Ph_2P-N=$

$PPh_2-PPh_2=N-PPh_2$ (**2**) as an impurity, but was nevertheless used for NMR experiments. Due to the low yield of the product [$*Pb_2\{(Ph_2P)_2N\}_2$] and its sensitivity to moisture, oxygen and various solvents we decided not to perform further purification. Yield 0.419 g (61%). The residue of the filtration consisted of traces of $Ph_2P-N=PPh_2-PPh_2=N-PPh_2$ (**2**) and LiCl that was detectable by $AgNO_3$ and flame spectrum.

Preparation of Tris[bis(diphenylphosphanyl)amido-P,P']-indium(3+) (**4**): To a solution of 1.49 g (3.87 mmol) of $HN(PPh_2)_2$ (**5**) in 50 ml of THF was added 2.60 ml (4.16 mmol) of *n*-butyllithium (1.6 M solution in *n*-hexane) and the mixture was stirred for 15 min at 20°C. Addition of 0.29 g of $InCl_3$ (1.29 mmol) resulted in a yellow suspension that turned into a clear yellow solution within 6 h. The solvent was removed in vacuo and the bright yellow residue was separated from LiCl by suspending it in 30 ml of benzene and filtering the mixture. The clear yellow filtrate was layered with 120 ml of *n*-pentane; after 48 h yellow crystals precipitated which were filtered off, washed with 5 ml of *n*-pentane and dried in vacuo, yielding 1.19 g (73%) of [$In\{(Ph_2P)_2N\}_3$], m.p. 182°C. – The crystals were suitable for an X-ray analysis. – ^1H NMR (C_6D_6, 21.5°C): δ = 7.65–6.60 (m, aromatic H), 3.55 (m, traces of THF), 3.02 (m, NH due to traces of moisture during sample preparation), 1.40 (m, traces of THF). – $^{13}C\{^1H\}$ NMR (C_4D_8O, 24.4°C): δ = 144.15 (m, C-*i*, Ph), 132.10 (pseudo-t, C-*o*, Ph), 129.05 (s, C-*p*, Ph), 128.75 (pseudo-t, C-*m*, Ph). – $^{31}P\{^1H\}$ NMR (C_6D_6, 22.0°C): δ = 80.06 (s); 40.74 [s, ≈ 5% of $(Ph_2P)_2NH$ due to traces of moisture during sample preparation]. – EI-MS (70 eV): *m/z* (%): 1270 (1.8) [$In\{HN(PPh_2)_2\}_3^+$], 385 (95) [$HN(PPh_2)_2^+$], 262 (95) [PPh_3^+]. – $C_{72}H_{60}InN_3P_6$ (1267.9): calcd. C 68.20, H 4.77, N 3.31; found C 67.54, H 5.15, N 2.89.

Table 2. Crystal data, data collection, and structure refinement for the complexes **3** and **4** (Siemens P4, Mo-K_α, 0.71073 A, graphite monochromator)

	3	**4**
Crystal data		
Formula	$C_{48}H_{40}N_2P_4Pb_2$	$C_{72}H_{60}InN_3P_6$
M_r	1183.08	1267.87
Crystal system	orthorhombic	orthorhombic
Space group	$P2_12_12_1$	$P2_12_12_1$
Crystal dimensions [mm]	0.80 × 0.60 × 0.60	0.50 × 0.30 × 0.20
a [pm]	1456.3(5)	1448.1(2)
b [pm]	3095 (1)	1452.6(5)
c [pm]	987.9(3)	2916.1(6)
α = β = γ [°]	90	90
V [nm^3]	4.453(3)	6.134(3)
Z	4	4
ρ_{calc} [gcm^{-3}]	1.765	1.373
F(000)	2264	2608
μ [mm^{-1}] Absorption coeff.	7.730	0.588
Data collection		
T [K]	293	200(2)
Scan mode	ω	ω
hkl range	$0 \le h \le 18$	$-1 \le h \le 18$
	$0 \le k \le 39$	$-1 \le k \le 18$
	$-12 \le l \le 7$	$-1 \le l \le 37$
Measured reflns.	6201	8835
Indep. reflns.	6030 (R_{int} = 0.0439)	8551 (R_{int} = 0.0462)
Observed reflns. [$F_o \ge 4.0\sigma(F)$]	3174	4073
Refinement	Full-matrix least-squares on F^2	
Data / Restraints / Parameter	6030 / 0 / 505	8551 / 0 / 739
Goodness-of-Fit on F^2	0.802[a]	0.704[a]
Final *R*-values	*R*1 = 0.0638[b]	*R*1 = 0.0459[b]
[$I < 2\sigma(I)$]	*wR*2 = 0.1539	*wR*2 = 0.0752
R-values (all data)	*R*1 = 0.0887	*R*1 = 0.1130
	*wR*2 = 0.1605[c]	*wR*2 = 0.0868[f]
Absolute structure parameter	0.03(2)[d]	−0.06(3)[d]
ρ_{fin}(*max*/*min*)(eÅ^{-3})	2.2233/−2.810[e]	0.756/−0.529

[a] GooF = $S = [\Sigma\{w(F_o^2 - F_c^2)^2\}/(n-p)]^{1/2}$ with n = 6030 (**3**), 8551 (**4**) and p = 505 (**3**), 739 (**4**). – [b] $R1 = [\Sigma(||F_o| - |F_c||/\Sigma|F_o|]$. – [c] $wR2 = [\Sigma\{w(F_o^2 - F_c^2)^2\}/\Sigma\{w(F_o^2)^2\}]^{1/2}$. – $w = 1/[\sigma^2(F_o^2)+(0.0950\cdot P)^2]$. – $P = (F_o^2)+2(F_c^2)/3$. – [d] H. D. Flack, *Acta Cryst.* **1983**, *A39*, 876–881. – [e] Residual electron densities (lower to 0.9 eÅ^{-3}) located close to the Pb atoms. – [f] $w = 1/[\sigma^2(F_o^2)]$.

Crystal Structure Determinations: Suitable single crystals of **3** and **4** were sealed into glass capillaries and used for measurement of precise cell constants and intensity data collection. Three standard reflections measured periodically during data collection showed no significant changes. Diffraction intensities were corrected for Lorentz and polarization effects. In the case of **3**, absorption effects were corrected empirically using Psi-scans of 40 reflections (min transmission = 0.002; max. transmission = 0.013). To minimize remaining absorption effects an additional correction using ΔF^2 methods[36] was applied (min. transmission = 0.089; max. transmission = 0.146). No absorption correction was applied in the case of **4**. The structures were solved by direct methods and refined by full-matrix least-squares calculations against F^2[37]. All non-hydrogen atoms were refined with anisotropic displacement parameters. The hydrogen atom positions of **3** and **4** were calculated and allowed to ride on their corresponding carbon atoms, their isotropic thermal parameters were tied to those of the adjacent carbon atoms by a factor of 1.5. Details of the crystal data, data collection, and structure refinement are summarized in Table 2. Crystallographic data (excluding structure factors) for the structures reported in this paper have been deposited with the Cambridge Crystallographic Data Centre as supplementary publication no. CCDC-100811. Copies of the data can be obtained free of charge on application to The Director, CCDC, 12 Union Road, Cambridge CB2 1EZ, UK [fax: int. code + 44(1223)336-033, e-mail: deposit@chemcrys.cam.ac.uk].

[1] J. Ellermann, M. Schütz, F. W. Heinemann, M. Moll, *Z. Anorg. Allg. Chem.* **1998**, *624*, 257–262.
[2] J. Ellermann, J. Sutter, F. A. Knoch, M. Moll, *Angew. Chem.* **1993**, *105*, 763–764; *Angew. Chem. Int. Ed. Engl.* **1993**, *32*, 700–701.
[3] J. Ellermann, J. Sutter, C. Schelle, F. A. Knoch, M. Moll, *Z. Anorg. Allg. Chem.* **1993**, *619*, 2006–2014.
[4] J. Ellermann, P. Gabold, C. Schelle, F. A. Knoch, M. Moll, W. Bauer, *Z. Anorg. Allg. Chem.* **1995**, *621*, 1832–1843.
[5] H. Schmidbaur, F. E. Wagner, A. Wohlleben-Hammer, *Chem. Ber.* **1979**, *112*, 496–500.
[6] J. Ellermann, M. Lietz, *Z. Naturforsch.* **1980**, *35b*, 64–67.
[7] A. Schmidpeter, F. Steinmüller, W. S. Sheldrick, *Z. Anorg. Allg. Chem.* **1989**, *579*, 158–172.
[8] Th. Kremer, F. Hampel, F. A. Knoch, W. Bauer, A. Schmidt, P. Gabold, M. Schütz, J. Ellermann, P. v. R. Schleyer, *Organometallics* **1996**, *15*, 4776–4782.
[9] P. Braunstein, R. Hasselbring, A. Tripicchio, F. Ugozzoli, *J. Chem. Soc., Chem. Commun.* **1995**, 37–38.
[10] J. Ellermann, P. Gabold, F. A. Knoch, M. Moll, A. Schmidt, M. Schütz, *Z. Naturforsch.* **1996**, *51b*, 201–208.
[11] M. Dotzler, A. Schmidt, J. Ellermann, F. A. Knoch, M. Moll, W. Bauer, *Polyhedron* **1996**, *15*, 4425–4433.
[12] A. F. Wells, *Structural Inorganic Chemistry*, 5th ed., Clarendon Press, Oxford, **1984**, p. 1279.
[13] M. Dräger, N. Kleiner in *Inorganic Reactions and Methods*, Vol.9: The Formation of Bonds to C, Si, Ge, Sn, Pb (Part 1), Founding Editor J. J. Zuckerman, Editor: A. P. Hagen, VCH, Weinheim, **1988**, p. 96–103.
[14] D. Pohl, J. Ellermann, F. A. Knoch, M. Moll, W. Bauer, *Chem. Ber.* **1994**, *127*, 2167–2171.
[15] D. Pohl, J. Ellermann, F. A. Knoch, M. Moll, W. Bauer, *J. Organomet. Chem.* **1994**, *481*, 259–274.

[16] J. Ellermann, P. Gabold, F. A. Knoch, M. Moll, D. Pohl, J. Sutter, W. Bauer, *J. Organomet. Chem.* **1996**, *525*, 89−107.
[17] B. Wrackmeyer in: G. A. Webb (Editor), *Annual Reports on NMR Spectroscopy*, Academic Press, London, **1990**, p. 249.
[18] M. Herberhold, V. Tröbs, B. Wrackmeyer, *J. Organomet. Chem.* **1997**, *541*, 391−400.
[19] J. D. Kennedy, W. McFarlane, B. Wrackmeyer, *Inorg. Chem.* **1976**, *15*, 1299−1302; J. D. Kennedy, W. McFarlane, G. S. Pyne, B. Wrackmeyer, *J. Organomet. Chem.* **1980**, *195*, 285−290.
[20] B. Wrackmeyer in: B. Krebs (Ed.), *Unkonventionelle Wechselwirkungen in der Chemie metallischer Elemente*, VCH, Weinheim, **1992**, 111−124.
[21] V. M. S. Gil, W. von Philipsborn, *Magn. Reson. Chem.* **1989**, *27*, 409−430.
[22] J. K. M. Sanders, B. K. Hunter, *Modern NMR Spectroscopy*, Oxford University Press, Oxford, **1993**, p. 214.
[23] H. H. Karsch, B. Deubelly, J. Riede, G. Müller, *Angew. Chem.* **1987**, *99*, 703−705; *Angew. Chem. Int. Ed. Engl.* **1987**, *26*, 673−675; H. H. Karsch, *Russ. Chem. Bull.* **1993**, *42*, 1937−1955.
[24] D. H. Whiffen, *J. Chem. Soc.* **1956**, 1350−1356.
[25] E. Maslowsky Jr., *Vibrational Spectra of Organometallic Compounds*, John Wiley and Sons, New York, London, Sydney, Toronto, **1977**, p. 399 and 402.
[26] M. J. S. Gynane, D. H. Harris, M. F. Lappert, P. P. Power, P. Riviere, M. Riviere-Baudet, *J. Chem. Soc., Dalton Trans.* **1977**, 2004−2009.
[27] D. H. Harris, M. F. Lappert, *J. Chem. Soc., Chem. Commun.* **1974**, 895−896.
[28] M. F. Lappert, P. P. Power, M. J. Slade, *J. Chem. Soc.,Chem. Commun.* **1979**, 369−370.
[29] J. S. Casa, A. Castineiras, J. Haiduc, A. Sanchez, J. Sordo, E. M. Velasquez-Lopez, *Polyhedron* **1994**, *13*, 2873−2879.
[30] A. L. Balch, D. E. Oram, *Organometallics* **1986**, *5*, 2159−2161.
[31] H. H. Karsch, A. Appelt, G. Hanika, *J. Organomet. Chem.* **1986**, *312*, C1−C5.
[32] A. L. Balch, D. E. Oram, *Inorg. Chem.* **1987**, *26*, 1906−1912.
[33] D. L. Kepert in *Progress in Inorganic Chemistry*, Vol. *23*, Aspects of the Stereochemistry of Six-coordination, Editor St. J. Lippart, John Wiley and Sons, New York, London, Sydney, Toronto, **1977**, p. 1−65.
[34] W. R. Krigbaum, B. Rubin, *Acta Cryst.* **1973**, *B29*, 749−756.
[35] H. Nöth, L. Meinel, *Z. Anorg. Allg. Chem.* **1967**, *349*, 225−240.
[36] S. Parkin, B. Moezzi, H. Hope, *J. Appl. Cryst.* **1995**, *28*, 53−56.
[37] SHELXTL 5.03 for Siemens Crystallographic Research Systems (**1995**), Siemens Analytical X-ray Instruments Inc., Madison, WI.

[97261]